ADVANCED MATERIALS INTERFACES

www.advmatinterfaces.de

Hydrothermally Reduced Graphene Oxide Interfaces for Synthesizing High-Performance Metal–Organic Framework Hollow Fiber Membranes

Wanbin Li, Jiali Shi, Zhanjun Li, Wufeng Wu, Yan Xia, Yang Yu, and Guoliang Zhang*

Metal–organic framework (MOF) membranes are attracting numerous attentions recently. However, fabrication of ultrathin and precisely molecular sieving MOF membranes, especially with highly processable polymeric hollow fiber substrates, is a great challenge. Here, the defect-free ZIF-8 composite hollow fiber membranes with impressive performance for hydrogen permselectivity are fabricated by novel interfacial contra-diffusion synthesis. The reduced graphene oxide (rGO) membranes with good selectivity are prepared on hollow fiber substrates via hydrothermal treatment. By employing the prepared rGO membranes as sharp interfaces to promote the heterogeneous nucleation and control the diffusion of precursors, the ultrathin and uniform MOF membranes with thickness of 150 nm can be regionally crystallized at interfaces by contra-diffusion synthesis. The prepared ZIF-8/rGO composite membranes display outstanding separation performance in H_2 purification, with permeance over 60×10^{-8} mol m^{-2} s^{-1} Pa^{-1} and H_2/CO_2, H_2/N_2 and H_2/CH_4 selectivities up to 25.3, 70.4, and 90.7, respectively. Moreover, the membranes thus prepared have good reproducibility and long-term stability.

Metal–organic frameworks (MOFs) have been applied for various applications including separation, adsorption, catalysis, and drug-delivery.[1–5] MOF membranes show great potential in the fields of gas separation, nanofiltration, and pervaporation.[6–16] High porosities and sharp pore sizes endow MOF membranes with superior permeability and selectivity than broadly used polymeric membranes. For separation application, both inorganic and polymeric substrates are employed to support MOF membranes.[6] Compared to inorganic substrates prepared by high-temperature calcination, polymeric substrates, especially polymeric hollow fibers, have been demonstrated with better competitiveness, in terms of processibility, cost, and membrane area per volume.[17–29] Various methods, such as in situ/secondary growth,[19–24] interfacial synthesis and contra-diffusion synthesis,[25–29] have been developed for achieving continuous MOF membranes. In these methods, interfacial and contra-diffusion synthesis have commendable implementation in fabrication of MOF hollow fiber membranes. Interfacial synthesis is performed by crystallization at interface of two immiscible solutions. While the issue of intermiscibility among solvents, metal salts, and ligands possibly hinders the development of interfacial synthesis more or less.[30] Contra-diffusion synthesis is executed by growth of MOF layers on substrates with two bilateral solutions. Although there is no requirement of immiscibility, the uncertain interface of two precursor solutions and the suddenly gush of one precursor into the other one should be carefully controlled. For improving heterogeneous nucleation and membrane continuity, the flat substrates with functional groups have been employed for contra-diffusion synthesis.[31,32] Moreover, for obtaining larger permeance, it is better to reduce the micrometer-sized thickness of the membranes derived from interfacial and contra-diffusion synthesis.

Graphene oxide (GO) membranes are proved with precisely molecular sieving properties for water and solvent treatments.[33–36] Nevertheless, for light–gas separation, GO membranes with different thicknesses display diverse features. Few-layered GO membranes exhibit both large permeance and selectivity,[37,38] micrometer-sized GO membranes are almost impermeable on contrary,[39] yet ultrathin GO membranes with thickness of hundreds of nanometers possess large permeance but moderate selectivity.[40,41] Despite the moderate performance, ultrathin GO membranes can be applied as interfaces for synthesizing MOF membranes. Wang used ZIF-8/GO hybrid nanosheets as seeds to prepare ZIF-8 membranes on anodic aluminum oxide (AAO) discs for molecular sieving.[42,43] Recently, we grew MOF nanosheets between reduced GO (rGO) sheets by in situ synthesis to transform impermeable rGO membranes to semipermeable composite membranes with

Prof. W. Li, J. Shi, Prof. Z. Li, W. Wu, Y. Xia, Prof. Y. Yu
Guangdong Key Laboratory of Environmental Pollution and Health and School of Environment
Jinan University
Guangzhou 510632, China
E-mail: gandeylin@126.com
Prof. G. Zhang
Institute of Oceanic and Environmental Chemical Engineering
State Key Lab Breeding Base of Green Chemical Synthesis Technology
Zhejiang University of Technology
Hangzhou 310014, China
The ORCID identification number(s) for the author(s) of this article can be found under https://doi.org/10.1002/admi.201800032.

DOI: 10.1002/admi.201800032

commendable selectivity.[44] If MOF membranes are prepared by contra-diffusion synthesis at ultrathin rGO interfaces on hollow fibers, the resulting membranes may have both higher permeance and larger selectivity.

Herein, we report an interfacial contra-diffusion synthesis to fabricate ultrathin MOF hollow fiber membranes for hydrogen purification by using rGO layers as interfaces. Hydrothermal synthesis is developed for obtaining the ultrathin rGO membranes on hollow fiber substrates. Because the ultrathin rGO layers promote the heterogeneous nucleation provide the sharp interfaces and control the diffusion of precursors, the defect-free MOF composite membranes can be regionally synthesized with nanoscale thickness. The formed MOFs in membranes can enhance gas permeance and selectivity substantively. The prepared MOF composite membranes display outstanding performance in separation of H_2 from CO_2, N_2, and CH_4.

Figure 1 shows the synthesis procedures of the ZIF-8/rGO membranes. The rGO membrane was first deposited on polyvinylidene fluoride (PVDF) hollow fiber. Ethylenediamine was employed to ammoniate PVDF hollow fiber for improving the stability and providing the amino groups.[17] For rGO deposition, the hollow fiber was immersed in GO suspension with various concentrations and subjected to thermal-treatment. During synthesis, the amino groups on the hollow fiber surface improved the deposition of GO with carboxyl groups through condensation reaction, meanwhile the hydrothermal treatment reduced GO to rGO. For comparison, the GO membranes with similar thickness were fabricated by vacuum filtration as previous studies.[33,35,36,39] Scanning electron microscopy (SEM) was employed to observe the morphologies of the obtained membranes. When the GO suspension with concentration of 0.2 mg mL^{-1} was applied, an ultrathin rGO layer with thickness of ≈70 nm was deposited on the hollow fiber surface (**Figure 2**a). With the decreasing of GO concentration from 1.0 mg mL^{-1} to 8.0 μg mL^{-1}, the thickness of the rGO layers reduced from about 3.3 μm to 13 nm (Figure S1, Supporting Information). Unlike the GO membranes with seamed interfaces between the deposited layers and the substrates (Figure 2b and Figure S2, Supporting Information), the rGO membranes with seamless interfaces showed better adhesion and compatibility because of the chemical interaction between the rGO layers and the hollow fibers. Chemical structures of the GO and the rGO were investigated by X-ray photoelectron spectroscopy (XPS) measurement. As shown in Figure 2c, C 1s spectrum of the GO showed intensive peaks for C—C, C—O, and C=O bonds, indicating the typical GO chemical structure. After hydrothermal treatment, the intensity of C—O and C=O bonds attenuated significantly, revealing the GO reduction. The decreasing of O content from 32.7 to 16.1% also proved the reduction (Figure S3, Supporting Information). Ramon spectra displayed the increased intensity ratio of D to G band, demonstrating the reduction of GO as well (Figure S4, Supporting Information).[35] X-ray diffraction (XRD) characterization indicated that the GO characteristic peak at 10.7° disappeared after thermal treatment, while a weak and broad peak at 24.5° appeared (Figure S5, Supporting Information). This result confirmed the GO reduction again and displayed the narrowing of the interlayer space. Gas permeances of the GO and rGO membranes were measured (Figure S6, Supporting Information). Like the observations in previous studies,[39,44] the rGO membrane with 3.3 μm thickness was impermeable. However, as shown in Figure 2d, the 70 nm rGO membrane showed H_2 permeance of 2.8×10^{-8} mol m^{-2} s^{-1} Pa^{-1}, with H_2/CO_2, H_2/O_2, H_2/N_2, and H_2/CH_4 ideal selectivities of 20.0, 11.6, 12.5, and 14.5, respectively. Compared to the GO membranes with ideal selectivities of 3.4 (H_2/CO_2), 2.6 (H_2/O_2), 3.0 (H_2/N_2), and 3.1 (H_2/CH_4), the rGO membrane had much better H_2 permselectivity. The higher selectivity of the rGO membrane was attributed to that the reduction of GO narrowed the interlayer space. As expected, for both GO and rGO membranes, the smaller thickness brought out higher permeance but lower selectivity (Figures S7 and S8, Supporting Information).

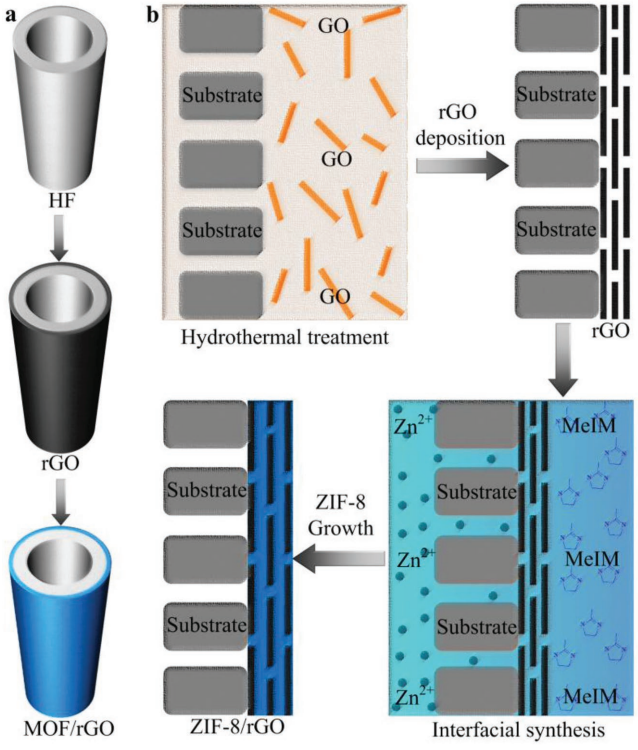

Figure 1. a) Schematic diagram for synthesizing MOF/rGO hollow fiber membranes. b) Crystallization of interfacial contra-diffusion synthesis of ZIF-8/rGO composite membranes.

The ZIF-8/rGO membranes were grown by interfacial contra-diffusion synthesis with tube-side metal salt solution and shell-side ligand solution. Because of the simultaneity of precursor diffusion and crystallization, the relative rates of these two processes were critical to the formation of defect-free membranes. When diffusion was faster than crystallization, the unconsumed precursor would enter into the other solution and react with the corresponding precursor to form bulk MOFs, thereby leading to formation of the uncontinuous membranes. Theoretically, faster crystallization than diffusion was beneficial to achieve dense MOF membranes.[45,46] Because of the residual oxygen-containing groups, the rGO layers could coordinate to zinc cation and then offer heterogeneous nucleation sites for MOF growth. As well as the mass transfer resistance from the rGO layer could greatly suppress the precursor diffusion to prevent the suddenly gush of one precursor solution into the other

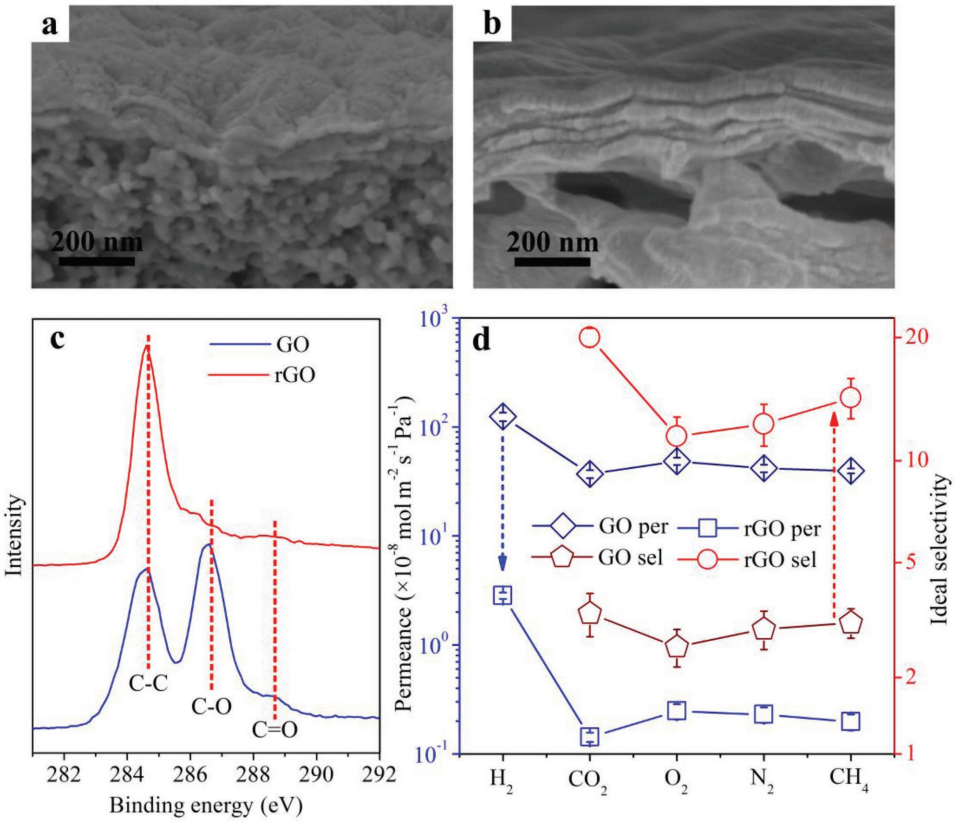

Figure 2. SEM images of a) the rGO hollow fiber membrane prepared by hydrothermal treatment and b) the GO membrane fabricated by vacuum filtration. c) High-resolution C 1s XPS spectra of the GO and the rGO. d) The permeation properties of various gases through the GO and rGO membranes.

one. The proposed interfacial contra-diffusion synthesis would be successfully employed for MOF membrane fabrication. XRD pattern of the formed composite membrane showed the characteristic peaks of ZIF-8 (Figure S9, Supporting Information). SEM images shown in **Figure 3**a revealed that the thickness of the membranes increased from 70 nm of the rGO membrane to 150 nm of the ZIF-8/rGO membrane. Comparatively, the ZIF-8/rGO membrane had a uniform 20 nm layer structure due to the formed stiff MOF nanosheets between the rGO sheets. The rGO membranes prepared with other concentrations were also exploited to fabricate the composite membranes (Figure S10, Supporting Information). The continuity of the composite membranes became worse as decreasing of GO concentration. The ZIF-8/rGO membrane prepared with GO concentration of 40 μg mL^{-1} possessed a heterogranular structure (Figure 3b). This could be explained by that the crystallization of ZIF-8 disturbed the arrangement of the rGO layer, which caused the formation of large diffusion channels and resulted in massive influx of one precursor into the other one. When 8.0 μg mL^{-1} of GO concentration was applied, because the stability of the rGO layer was too low to against the shear force from MOF crystallization, the prepared composite membrane was uncontinuous. The morphologies of the ZIF-8 particles in the fingerlike structures of the hollow fibers were investigated (Figure S11, Supporting Information). With the increase of GO concentration, the polyhedral particles with two exposed facets of (100) and (110) were transformed to the cubic particles with one exposed facet of (100). This preferred growth was interpreted by that the different ligand/Zn ratios were suited to synthesis of different MOF particles. Because the increased rGO thickness reduced the ligand diffusion rate, the ligand/Zn ratio in PVDF hollow fibers decreased as increased GO concentration. Transmission electron microscopy (TEM) images of the composite membranes were collected (Figure 3c,d and Figure S12, Supporting Information). As similar to the observation in SEM images, the composite membrane prepared with GO concentration of 0.2 mg mL^{-1} showed a flat nanosheet structure, while the membrane prepared with concentration of 40 μg mL^{-1} possessed a particle structure that was wrapped by rGO.

The permeation of various gases through the prepared ZIF-8/rGO hollow fiber membranes was investigated. **Figure 4**a presents the single-component permeance as the function of gas kinetic diameter. The membrane exhibited a decreasing permeance order as the increased kinetic diameter, and showed largest H_2 permeance of 67.9×10^{-8} mol m^{-2} s^{-1} Pa^{-1}. The H_2/CO_2, H_2/O_2, H_2/N_2, and H_2/CH_4 ideal selectivities of the ZIF-8/rGO membrane with GO concentration of 0.2 mg mL^{-1} were 25.0, 42.3, 66.4, and 83.3, respectively. These values were much greater than the Knudsen diffusion selectivities of 4.7 (H_2/CO_2), 4.0 (H_2/O_2), 3.7 (H_2/N_2), and 2.8 (H_2/CH_4), demonstrating the precisely molecular sieving property. The permeation properties of the membranes prepared with other GO concentrations were also studied (Figures S13–S15, Supporting Information). The decrease of GO concentration enhanced permeance but

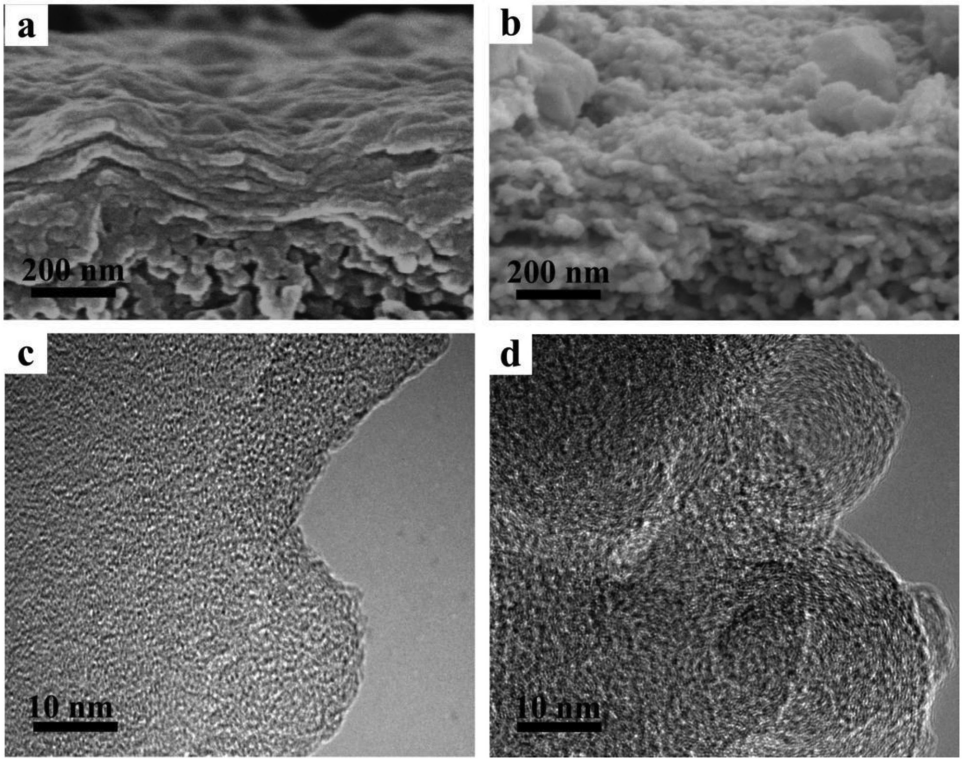

Figure 3. SEM images of the ZIF-8/rGO membranes prepared with GO concentrations of a) 0.2 mg mL^{-1} and b) 40 μg mL^{-1}. TEM images of the ZIF-8/rGO membranes prepared with GO concentrations of c) 0.2 mg mL^{-1} and d) 40 μg mL^{-1}.

weakened selectivity. This phenomenon was consistent with the change of membrane structures, ZIF-8 crystallization disturbed the arrangement of the membranes prepared with low GO concentrations. For investigating the separation performance, the rGO and ZIF-8/rGO membranes prepared with GO concentration of 0.2 mg mL^{-1} were employed to separate H_2/CO_2, H_2/N_2, and H_2/CH_4 binary mixtures (Figure 4b and Figure S16, Supporting Information). Compared to the single-component permeation, both the membranes showed slightly smaller permeance and selectivity due to the competitive adsorption of two feed gases to selective layer. While H_2/CO_2, H_2/N_2, and H_2/CH_4 selectivities of ZIF-8/rGO membrane still reached as high as 23.3, 63.3, and 80.9, respectively, accompanying with H_2 permeance over 60×10^{-8} mol m^{-2} s^{-1} Pa^{-1}. The similar separation performance of the three membrane samples prepared with same procedures indicated the good reproducibility of the synthesis methods (Figure 4c,d). Moreover, the long-term separation performance of H_2/CH_4 binary mixture through the ZIF-8/rGO membrane was investigated (Figure S17, Supporting Information). The small fluctuations of gas permeance and selectivity over 48 h revealed the good long-time stability of the prepared membrane.

Comparing GO, rGO, and ZIF-8/rGO membranes prepared in this study, it was obvious that the ZIF-8/rGO membrane exhibited best separation performance, while the GO membrane prepared by vacuum filtration showed highest permeance but lowest selectivity. For H_2/N_2 and H_2/CH_4 separations (Figure 4c,d), the selectivities of the rGO membrane increased to 4.2–4.6 times of those of the GO membrane, but the permeance decreased vastly due to the narrowed interlayer space. After crystallization, the selectivities of ZIF-8/rGO membrane further increased to 5.8–6.3 times as the rGO membrane, the permeance simultaneously increased by 21 times and closed to the values of the GO membrane. For H_2/CO_2 separation, the three membranes showed a similar tendency as for H_2/N_2 and H_2/CH_4 mixtures, expectation of 1.4 times of increase in selectivity from the rGO membrane to the ZIF-8/rGO membrane (Figure S18, Supporting Information). This should be interpreted by the difference in separation mechanism of the different membranes. In membrane-based gas separation, the separation mechanism can be mainly classified into two kinds, solution-diffusion and molecular sieving.[47,48] Because of the sub-nanometer-sized interlayer space of rGO and the microporous structure of ZIF-8, the molecular sieving was the dominated mechanism in this study. The larger H_2/CO_2 selectivity of 17.2 but smaller H_2/N_2 (10.8) and H_2/CH_4 (12.9) ones of the rGO membrane should be caused by that the strong affinity of residual oxygen-containing groups to CO_2 molecules suppressed their diffusion rate (Figure S16, Supporting Information). In respect to the ZIF-8/rGO membrane, because of the formation of porous ZIF-8, all gas permeances increased dramatically. This phenomenon revealed that the main transport channels were changed from interlayer spaces of rGO to the pores of ZIF-8 (Figure S19, Supporting Information). Since the theoretical 0.34 nm pore of ZIF-8 was smaller than N_2 (0.364 nm) and CH_4 (0.38 nm), similar to CO_2 (0.33 nm) and bigger than H_2 (0.289 nm), the larger gas showed lower increase due to the molecular sieving effect. Therefore,

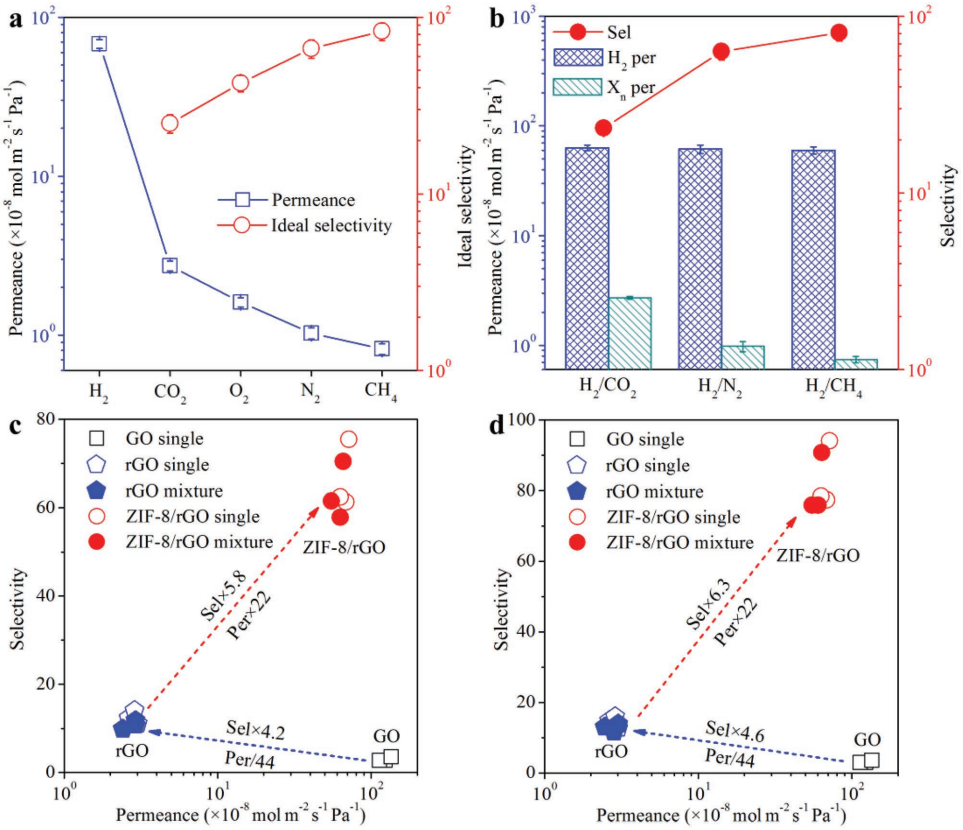

Figure 4. a) The permeation properties of various gases through the ZIF-8/rGO membrane. b) The separation performance of the ZIF-8/rGO membrane for H_2/CO_2, H_2/N_2, and H_2/CH_4 mixtures. The comparison of the GO, rGO, and ZIF-8/rGO membranes for c) H_2/N_2 and d) H_2/CH_4 separations.

the ZIF-8/rGO membrane exhibited the increasing selectively order as H_2/CO_2, H_2/N_2, and H_2/CH_4. The permeation of N_2 and CH_4 through the membrane was the result of the flexibility of ZIF-8.[49]

ZIF-8 membranes have been widely fabricated and applied for gas separation. Huang and co-workers fabricated a ZIF-8 membrane with H_2 permeance of 18×10^{-8} mol m^{-2} s^{-1} Pa^{-1}, meanwhile with good H_2/CO_2 (8.9), H_2/N_2 (16.2), and H_2/CH_4 (31.5) selectivities.[50] Besides pure membranes, ZIF-8 membranes were hybridized by other matters to improve the selectivity. Liu et al. reported a ZIF-8-ZnAl-NO_3 membrane with excellent H_2/N_2-H_2/CH_4 selectivities of 16.8–54.1 and H_2 permeance of 4.1×10^{-8} mol m^{-2} s^{-1} Pa^{-1}.[51] The ZIF-8/GO composite membrane prepared by Wang and co-workers exhibited H_2 permeance of 5.5×10^{-8} mol m^{-2} s^{-1} Pa^{-1} and ideal selectivities of 11.1 for H_2/N_2 and 11.2 for H_2/CH_4.[42] For improving the permeance, the same group synthesized the ZIF-8/GO composite membrane with mesoporous GO, which had high H_2 permeance of 118×10^{-8} mol m^{-2} s^{-1} Pa^{-1} and ideal selectivities of 10.0 for H_2/N_2 and 10.4 for H_2/CH_4.[43] Compared with those high-performance ZIF-8 membranes reported in previous studies,[6] our membranes showed impressive separation performance, with H_2 permeance over 60×10^{-8} mol m^{-2} s^{-1} Pa^{-1}, and selectivities up to 25.3 (H_2/CO_2), 70.4 (H_2/N_2), and 90.7 (H_2/CH_4) (Figure 4c,d and Figure S18, Supporting Information). The outstanding selectivity may be partially attributed to the suppression of framework flexibility from the combined rGO.[52] The low cost and large area per volume of hollow fiber substrates would further increase the competitiveness of the prepared membranes in this study. More recently, we in situ synthesized the ZIF-8/rGO composite membrane with H_2/CO_2 selectivity of 18.8 and H_2 permeance of 0.7×10^{-8} mol m^{-2} s^{-1} Pa^{-1}.[44] Because interfacial contra-diffusion synthesis formed more ZIF-8 phase originating from the additional zinc cation in tube-side solution and could preferentially grow the framework at the potential defects of the membranes, as well as the thickness was ultrathin, the ZIF-8/rGO membrane here displayed superior selectivity and about two orders of magnitude higher permeance than the in situ synthesized ZIF-8/rGO membrane. In gas separation, the Robeson upper bound relationships of polymeric membranes between the selectivity and permeability are good standards to judge the membrane performance.[53] For all H_2/CO_2, H_2/N_2, and H_2/CH_4 systems, the separation performance of our ZIF-8/rGO membrane exceeded the Robeson upper bounds easily (Figure S20, Supporting Information).

In conclusion, we have reported a novel interfacial contra-diffusion synthesis strategy for fabricating ZIF-8/rGO membranes with high performance in H_2 purification. We found that the narrowed rGO membranes with good selectivity could be synthesized via hydrothermal treatment. By employing the rGO layers to provide heterogeneous nucleation sites, supply sharp interfaces, and reduce precursor diffusions, the ultrathin ZIF-8/rGO membranes could be restrictively prepared without defects. The prepared ZIF-8/rGO membranes showed H_2/CO_2,

H_2/N_2, and H_2/CH_4 selectivities up to 25.3, 70.4, and 90.7, respectively, meanwhile with large H_2 permeance over 60×10^{-7} mol m^{-2} s^{-1} Pa^{-1}. Moreover, the prepared membrane displayed good reproducibility and long-term stability. Overall, the developed ZIF-8/rGO membranes offer an alternative concept for designing ultrathin hollow fiber membranes with unique gas separation.

Supporting Information

Supporting Information is available from the Wiley Online Library or from the author.

Acknowledgements

This work was financially supported by the National Natural Science Foundation of China (Grant No. 51708252), the Fundamental Research Funds for the Central Universities (Grant No. 21617322), and Jinan University (Grant No. 88016674).

Conflict of Interest

The authors declare no conflict of interest.

Keywords

graphene oxides, hydrogen purification, interfacial synthesis, metal–organic frameworks, ultrathin membranes

Received: January 8, 2018
Revised: March 14, 2018
Published online: May 3, 2018

[1] H. Furukawa, K. E. Cordova, M. O'Keeffe, O. M. Yaghi, *Science* **2013**, *341*, 1230444.
[2] M. S. Denny, J. C. Moreton, L. Benz, S. M. Cohen, *Nat. Rev. Mater.* **2016**, *1*, 16078.
[3] Y. Y. Zhang, S. Yuan, X. Feng, H. W. Li, J. W. Zhou, B. Wang, *J. Am. Chem. Soc.* **2016**, *138*, 5785.
[4] Y. Yu, X. J. Wu, M. Zhao, Q. Ma, J. Chen, B. Chen, M. Sindoro, J. Yang, S. K. Han, Q. P. Lu, H. Zhang, *Angew. Chem., Int. Ed.* **2017**, *56*, 578.
[5] S. Beyer, R. Schürmann, I. Feldmann, A. Blocki, I. Bald, R. J. Schneider, F. Emmerling, *Colloid Interface Sci. Commun.* **2018**, *22*, 14.
[6] W. Li, Y. Zhang, Q. Li, G. Zhang, *Chem. Eng. Sci.* **2015**, *135*, 232.
[7] Y. Liu, Y. Ban, W. Yang, *Adv. Mater.* **2017**, *29*, 1606949.
[8] F. Zhang, X. Zo, X. Gao, S. Fan, F. Sun, H. Ren, G. Zhu, *Adv. Funct. Mater.* **2012**, *22*, 3583.
[9] Z. Kang, M. Xue, L. Fan, L. Huang, L. Guo, G. Wei, B. Chen, S. Qiu, *Energy Environ. Sci.* **2014**, *7*, 4053.
[10] Y. Peng, Y. S. Li, Y. J. Ban, H. Jin, W. M. Jiao, X. L. Liu, W. S. Yang, *Science* **2014**, *346*, 1356.
[11] Y. Sun, F. Yang, Q. Wei, N. Wang, X. Qin, S. Zhang, B. Wang, Z. Nie, S. Ji, H. Yan, J. R. Li, *Adv. Mater.* **2016**, *28*, 2374.
[12] Y. Peng, Y. Li, Y. Ban, W. Yang, *Angew. Chem., Int. Ed.* **2017**, *56*, 9757.
[13] A. Knebel, B. Geppert, K. Volgmann, D. I. Kolokolov, A. G. Stepanov, J. Twiefel, P. Heitjans, D. Volkmer, J. Caro, *Science* **2017**, *358*, 347.
[14] M. J. Lee, H. T. Kwon, H. K. Jeong, *Angew. Chem., Int. Ed.* **2018**, *57*, 156.
[15] X. Liu, N. K. Demir, Z. Wu, K. Li, *J. Am. Chem. Soc.* **2015**, *137*, 6999.
[16] X. Liu, C. Wang, B. Wang, K. Li, *Adv. Funct. Mater.* **2017**, *27*, 1604311.
[17] W. Li, P. Su, Z. Li, Z. Xu, F. Wang, H. Ou, J. Zhang, G. Zhang, E. Zeng, *Nat. Commun.* **2017**, *8*, 406.
[18] Y. Mao, J. Li, W. Cao, Y. Ying, L. Sun, X. Peng, *ACS Appl. Mater. Interfaces* **2014**, *6*, 4473.
[19] A. J. Brown, J. R. Johnson, M. E. Lydon, W. J. Koros, C. W. Jones, S. Nair, *Angew. Chem., Int. Ed.* **2012**, *51*, 10615.
[20] W. Li, G. Zhang, C. Zhang, Q. Meng, Z. Fan, C. Gao, *Chem. Commun.* **2014**, *50*, 3214.
[21] F. Cacho-Bailo, G. Caro, M. Etxeberría-Benavides, O. Karvan, C. Téllez, J. Coronas, *Chem. Commun.* **2015**, *51*, 11283.
[22] W. Li, Y. Zhang, C. Zhang, Q. Meng, Z. Xu, P. Su, Q. Li, C. Shen, Z. Fan, L. Qin, G. Zhang, *Nat. Commun.* **2016**, *7*, 11315.
[23] J. Hou, P. D. Sutrisna, Y. Zhang, V. Chen, *Angew. Chem., Int. Ed.* **2016**, *55*, 3947.
[24] F. Cacho-Bailo, I. Matito-Martos, J. Perez-Carbajo, M. Etxeberría-Benavides, O. Karvan, V. Sebastián, S. Calero, C. Télleza, J. Coronas, *Chem. Sci.* **2017**, *8*, 3253.
[25] A. M. Marti, W. Wickramanayake, G. Dahe, A. Sekizkardes, T. L. Bank, D. P. Hopkinson, S. R. Venna, *ACS Appl. Mater. Interfaces* **2017**, *7*, 5678.
[26] A. J. Brown, N. A. Brunelli, K. Eum, F. Rashidi, J. R. Johnson, W. J. Koros, C. W. Jones, S. Nair, *Science* **2014**, *345*, 72.
[27] B. P. Biswal, A. Bhaskar, R. Banerjee, U. K. Kharul, *Nanoscale* **2015**, *7*, 7291.
[28] K. Eum, A. Rownaghi, D. Choi, R. R. Bhave, C. W. Jones, S. Nair, *Adv. Funct. Mater.* **2016**, *26*, 5011.
[29] K. Eum, C. Ma, A. Rownaghi, C. W. Jones, S. Nair, *ACS Appl. Mater. Interfaces* **2016**, *8*, 25337.
[30] A. Carné-Sánchez, I. Imaz, M. Cano-Sarabia, D. Maspoch, *Nat. Chem.* **2013**, *5*, 203.
[31] E. Shamsaei, X. Lin, Z. X. Low, Z. Abbasi, Y. Hu, J. Z. Liu, H. Wang, *ACS Appl. Mater. Interfaces* **2016**, *8*, 6236.
[32] E. Barankova, X. Tan, L. F. Villalobos, E. Litwiller, K. V. Peinemann, *Angew. Chem., Int. Ed.* **2017**, *56*, 2965.
[33] R. K. Joshi, P. Carbone, F. C. Wang, V. G. Kravets, Y. Su, I. V. Grigorieva, H. A. Wu, A. K. Geim, R. R. Nair, *Science* **2014**, *343*, 752.
[34] L. Chen, G. Shi, J. Shen, B. Peng, B. Zhang, Y. Wang, F. Bian, J. Wang, D. Li, Z. Qian, G. Xu, G. Liu, J. Zeng, L. Zhang, Y. Yang, G. Zhou, M. Wu, W. Jin, J. Li, H. Fang, *Nature* **2017**, *550*, 380.
[35] L. Huang, J. Chen, T. Gao, M. Zhang, Y. Li, L. Dai, L. Qu, G. Shi, *Adv. Mater.* **2016**, *28*, 8669.
[36] Q. Yang, Y. Su, C. Chi, C. T. Cherian, K. Huang, V. G. Kravets, F. C. Wang, J. C. Zhang, A. Pratt, A. N. Grigorenko, F. Guinea, A. K. Geim, R. R. Nair, *Nat. Mater.* **2017**, *16*, 1198.
[37] H. Li, Z. Song, X. Zhang, Y. Huang, S. Li, Y. Mao, H. J. Ploehn, Y. Bao, M. Yu, *Science* **2013**, *342*, 95.
[38] H. W. Kim, H. W. Yoon, S. M. Yoon, B. M. Yoo, B. K. Ahn, Y. H. Cho, H. J. Shin, H. Yang, U. Paik, S. Kwon, J. Y. Choi, H. B. Park, *Science* **2013**, *342*, 91.
[39] R. R. Nair, H. A. Wu, P. N. Jayaram, I. V. Grigorieva, A. K. Geim, *Science* **2012**, *335*, 442.
[40] J. Shen, G. Liu, K. Huang, Z. Chu, W. Jin, N. Xu, *ACS Nano* **2016**, *10*, 3398.
[41] X. Wang, C. Chi, J. Tao, Y. Peng, S. Ying, Y. Qian, J. Dong, Z. Hu, Y. Gu, D. Zhao, *Chem. Commun.* **2016**, *52*, 8087.
[42] Y. Hu, J. Wei, Y. Liang, H. Zhang, X. Zhang, W. Shen, H. Wang, *Angew. Chem., Int. Ed.* **2016**, *55*, 2048.
[43] Y. Hu, Y. Wu, C. Devendran, J. Wei, Y. Liang, M. Matsukata, W. Shen, A. Neild, H. Huang, H. Wang, *J. Mater. Chem. A* **2017**, *5*, 16255.
[44] W. Li, Y. Zhang, P. Su, Z. Xu, G. Zhang, C. Shen, Q. Meng, *J. Mater. Chem. A* **2016**, *4*, 18747.

[45] H. T. Kwon, H. K. Jeong, *J. Am. Chem. Soc.* **2013**, *135*, 10763.
[46] W. Li, Y. Zhang, Z. Xu, Q. Meng, Z. Fan, S. Ye, G. Zhang, *Angew. Chem., Int. Ed.* **2016**, *55*, 955.
[47] J. Yao, H. Wang, *Chem. Soc. Rev.* **2014**, *43*, 4470.
[48] K. J. Berean, J. Z. Ou, M. Nour, M. R. Field, M. M. Y. A. Alsaif, Y. Wang, R. Ramanathan, V. Bansal, S. Kentish, C. M. Doherty, A. J. Hill, C. McSweeney, R. B. Kaner, K. Kalantar-zadeh, *J. Phys. Chem. C* **2015**, *119*, 13700.
[49] C. Zhang, R. P. Lively, K. Zhang, J. R. Johnson, O. Karvan, W. J. Koros, *J. Phys. Chem. Lett.* **2012**, *3*, 2130.
[50] Q. Liu, N. Wang, J. Caro, A. Huang, *J. Am. Chem. Soc.* **2013**, *135*, 17679.
[51] Y. Liu, J. H. Pan, N. Wang, F. Steinbach, X. Liu, J. Caro, *Angew. Chem., Int. Ed.* **2015**, *54*, 3028.
[52] Y. Liu, Y. Peng, N. Wang, Y. Li, J. H. Pan, W. Yang, J. Caro, *ChemSusChem* **2015**, *8*, 3582.
[53] L. M. Robeson, *J. Membr. Sci.* **2008**, *320*, 390.

